Local Growth of Graphene by Ion Implantation of Carbon in a Nickel Thin Film followed by Rapid Thermal Annealing

Jeong Hun Mun, Sung Kyu Lim and Byung Jin Cho

J. Electrochem. Soc. 2012, Volume 159, Issue 6, Pages G89-G92.
doi: 10.1149/2.059206jes

Journal of The Electrochemical Society, **159** (6) G89-G92 (2012)
0013-4651/2012/159(6)/G89/4/$28.00 © The Electrochemical Society

Local Growth of Graphene by Ion Implantation of Carbon in a Nickel Thin Film followed by Rapid Thermal Annealing

Jeong Hun Mun,[a] Sung Kyu Lim,[b] and Byung Jin Cho[a,z]

[a]*Department of Electrical Engineering, KAIST, Yuseong-gu, Daejeon 305-701 Korea*
[b]*National NanoFab Center, Yuseong-gu, Daejeon 305-701, Korea*

Carbon ions were implanted in a nickel thin film. After subsequent rapid thermal annealing, they segregated on the surface, forming a graphene layer. The dependence of graphene synthesis on process conditions, including the carbon implantation dose, RTA temperature, and time, were investigated. The graphene shows quality comparable to that of the best reported CVD graphene. It was also found that local growth of graphene through local implantation requires stringent control of the process chamber conditions in order to avoid growth of graphene on unimplanted regions.

Manuscript submitted January 23, 2012; revised manuscript received March 6, 2012. Published April 30, 2012.

Graphene is a one-atom-thick planar material that has a two-dimensional hexagonal lattice with a sp2 hybridized carbon bond network. Due to its outstanding electrical properties, such as its high carrier mobility,[1–4] graphene has garnered great attention as a candidate material for future electronic devices. However, the synthesis of high-quality, wafer-scale graphene remains one of the principal challenges in the realization of graphene-based electronics. Among the various graphene synthesis methods, chemical vapor deposition (CVD) methods on catalytic metals such as polycrystalline thin film nickel or copper show feasibility for large-scale fabrication with acceptable levels of quality.[5–12] As graphene is a mono-atomic layer material, however, control of the thickness uniformity and reproducibility of the CVD process are very challenging, as the growth of graphene using CVD is sensitive to such factors as the chamber size, gas flow rate, decomposition rate of the hydrocarbon, and process history of the chamber. Such problems originate from the use of hydrocarbon gas as a carbon source, which makes it difficult to control the amount of carbon atoms exposed to the catalytic metal surface. From this point of view, various attempts to synthesize graphene layers, including the use of solid carbon sources[13–15] or amorphous carbon,[16] as well as the implantation of carbon ions[17,18] have been introduced. Among these methods, carbon ion implantation has strong potential for electronic device application because the ion implantation process is the most precise, reliable, and reproducible processing technique currently being used in commercial semiconductor chip fabrication. However, the detailed synthesis mechanism and process dependency of graphene growth by carbon ion implantation have not been well studied. In this work, graphene growth on nickel film using carbon ion implantation and subsequent annealing is investigated, focusing on the dependence of the process conditions for the graphene growth, including annealing condition, implantation dose, and gas ambient.

Experimental

Fig. 1a presents a brief illustration of the process sequence for graphene synthesis by ion implantation. A 300-nm thick nickel thin film is deposited onto a SiO_2/Si substrate followed by annealing in a H_2/Ar ambient at 1 atm at 1000°C for 10 min for crystallization of the deposited nickel thin film. The implantation dose and energy are selected with consideration of the implanted carbon profile and the solid solubility of the carbon in the nickel, as respectively shown in Figs. 1b and 1c. The profiles of carbon implanted in the nickel film at an implantation dose range of $1 \times 10^{14} \sim 10^{16}$ /cm^2 and an energy range of 40 ∼ 120 keV are shown in Figs. 1b and 1c, respectively; these values were calculated using the commercial simulator SRIM 2003. It was considered that the projection range (Rp) should be as shallow as possible for easy diffusion and segregation of the carbon to the nickel surface. In this experiment, we fixed the implantation energy at 40 keV, corresponding with the lowest practically possible implantation energy of our implanter; these conditions led to a reasonably shallow Rp of 500 Å. The implantation dose was varied from 1×10^{13} to 5×10^{15} /cm^2 to investigate the relationship between the implantation dose and the thickness of the synthesized graphene layers. After carbon ion implantation, the wafer was subjected to rapid thermal annealing (RTA) in 10% H_2/Ar ambient with a pressure of 800 mTorr for 5 ∼ 1800 sec at 600 ∼ 800°C for segregation of the carbon. Both the heating and cooling rates during post-implantation RTA were 10°C/sec. The graphene layer formed on the nickel surface was then transferred onto another SiO_2 (100 nm)/Si substrate using poly(methyl methacrylate) (PMMA) and wet-etching of the nickel thin film; this method is similar to the technique conventionally used for the transfer of CVD grown graphene on metal substrates.[6–8]

The thickness and quality of graphene layers were estimated by Raman spectroscopy (HR800, Horiba Jobin-Yvon) excited at 514 nm. Sample morphologies were examined with an atomic force microscope (XE-100, Park System) and a scanning tunneling microscope (D-3100, Veeco). The sheet resistance and Hall mobility were measured with a Hall effect measurement system (HMS-3000, Ecopia). All morphological and electrical characterizations were performed

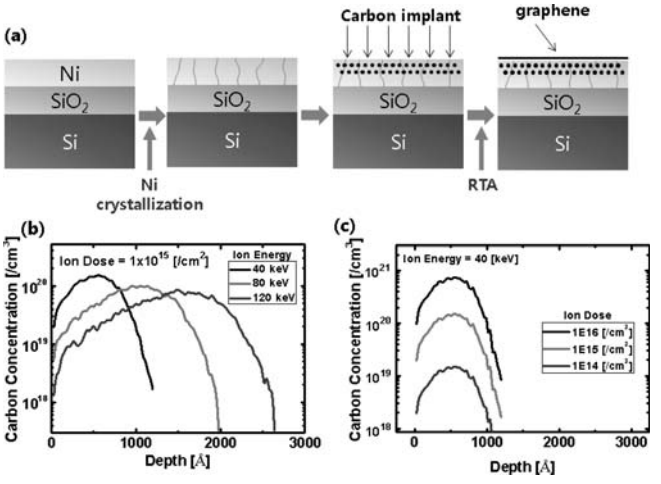

Figure 1. (a) Graphene synthesis procedure by carbon implantation and subsequent RTA. (b) Carbon concentration profiles in nickel for different carbon ion implantation energy levels when the carbon ion dose is fixed at 1×10^{15}/cm^2. The profiles were calculated using the SRIM2003 simulator. The projection range, Rp, of the carbon in the nickel is roughly 500 Å at an implantation energy level of 40 keV. (c) Carbon concentration profiles in nickel for different carbon ion implantation doses when the carbon ion energy is fixed at 40 keV.

[z]E-mail: bjcho@ee.kaist.ac.kr

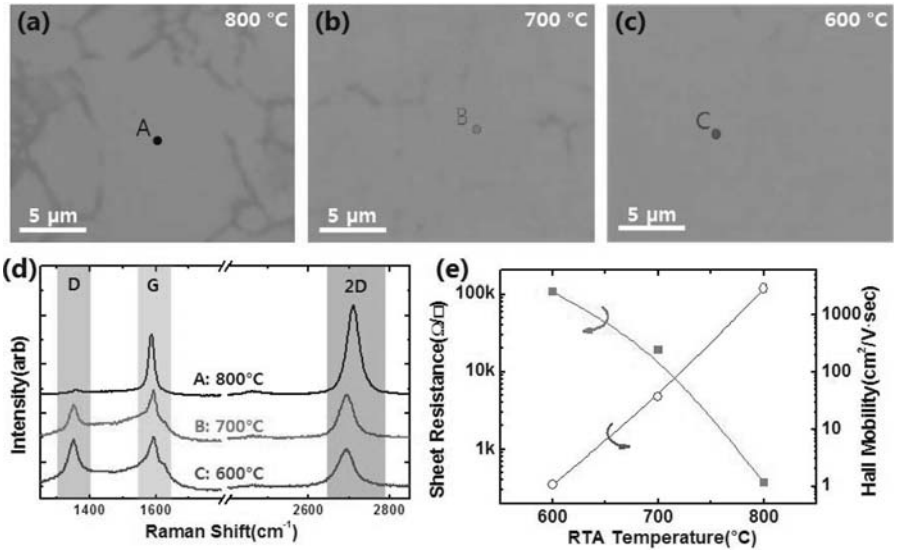

Figure 2. Optical microscope images of transferred graphene layers on SiO_2/Si, synthesized by carbon implantation followed by RTA at (a) 800°C, (b) 700°C, and (c) 600°C. (d) Raman spectra measured on the spots denoted as A-C in the microscope images. (e) Sheet resistance and Hall mobility of synthesized graphene as a function of the RTA temperature. The RTA time here was 300 sec.

after the transfer of the synthesized graphene layers onto the SiO_2 (100 nm)/Si substrates.

Results and Discussion

The effect of the post-implantation RTA temperature was initially investigated. Optical microscope images of transferred graphene layers synthesized at an RTA temperature in a range of 600–800°C at an RTA time of 300 sec and an implantation dose of 1×10^{15} /cm^2 are shown in Figs. 2a–2c. The results show that a high-quality mono-layer graphene layer was successfully synthesized on a sample at 800°C RTA, as confirmed by the Raman spectra presented in Fig. 2d.[19,20] In the sample prepared at 800°C RTA, slightly thicker graphene layers were also observed along the grain boundaries of the nickel thin film, indicating a higher amount of carbon segregation at the grain boundary region. Such non-uniform growth along the grain boundary diminishes as the RTA temperature decreases, as shown in Figs. 2b and 2c. However, the graphene layers segregated at lower RTA temperatures are more defective, as indicated by the increase of the D band in the Raman spectra shown in Fig. 2d. The trends in the sheet resistance and Hall mobility in Fig. 2e also present good agreement with the results of the Raman spectra in Fig. 2d. As the RTA temperature increases, the sheet resistance (red filled square) decreases while the Hall mobility (blue empty circle) increases, indicating that the graphene segregated at higher temperatures has better quality. At RTA at 800°C, the Hall mobility and sheet resistance of the monolayer graphene approach 2916 cm^2/V•sec and 370 Ω/□, respectively, reflecting a quality level similar to that of the best CVD grown graphene reported to date.[5–10]

To find a means of reducing the excessive carbon segregation along the grain boundary while maintaining the RTA temperature at 800°C, the dependence of the RTA time was investigated. Fig. 3a shows the trend of the intensity ratio of the D, G, and 2D bands, (I_D/I_G, I_G/I_{2D}), from the Raman spectra of the graphene. The I_G/I_{2D} intensity ratio, which depends on the thickness of the graphene layer, decreases with a decrease in the RTA time. The I_D/I_G ratio, which indicates the number of defects in the graphene layer, rapidly increases when the RTA time is less than 10 sec. This likely originates from incomplete coverage of the graphene on the nickel surface, which in turn leads to a large amount of graphene edges. The sheet resistance decreases monotonically with the RTA time and eventually saturates at ~370 Ω/□. However, the Hall mobility initially increases with the RTA time and then decreases upon long RTA time. The decreased mobility with long RTA time is attributed to the formation of multilayer graphene; this result also coincides closely with other data in the figure. A peak mobility of ~2900 cm^2/V · sec is obtained when the RTA time is in a range of 200–300 sec. To characterize the effect of the implant dose, the thicknesses of the synthesized graphene layers were investigated for a wide range of implantation doses, from 1×10^{13} to 5×10^{15} /cm^2. The RTA time was also simultaneously varied from 5 to 300 sec and the RTA temperature was fixed at 800°C. As shown in Fig. 4, the thickness of the graphene layer increases monotonously with the implant dose. However, the change of thickness according to variation of the implantation dose is much smaller than expected. For example, at a RTA time of 300 sec, when the implantation dose is decreased by two orders of magnitude (from 1×10^{15} to 1×10^{13} /cm^2), the thickness is only reduced by 29% (from 2.4 to 1.7 nm). It should also be noted that the RTA time has a much stronger effect on the graphene

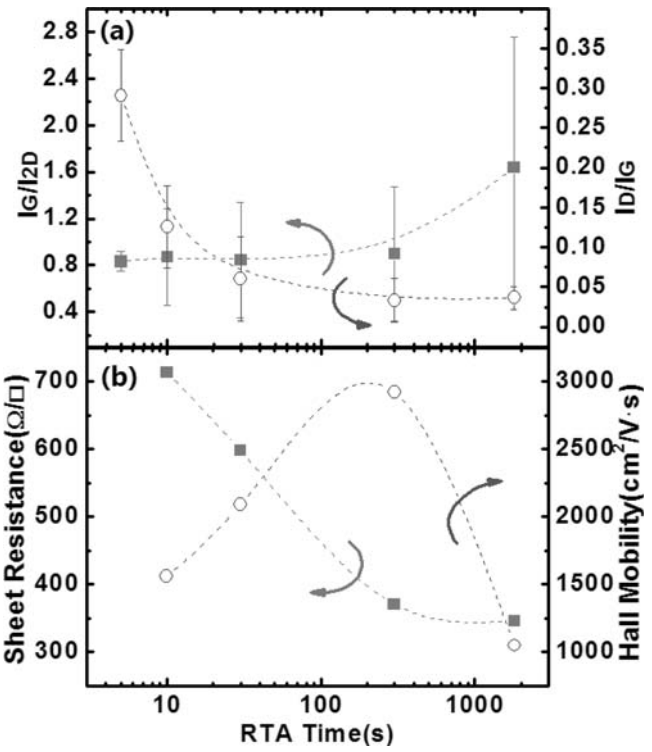

Figure 3. (a) Raman peak ratio (I_G/I_{2D} and I_D/I_G) and (b) sheet resistance and Hall mobility in terms of various RTA time.

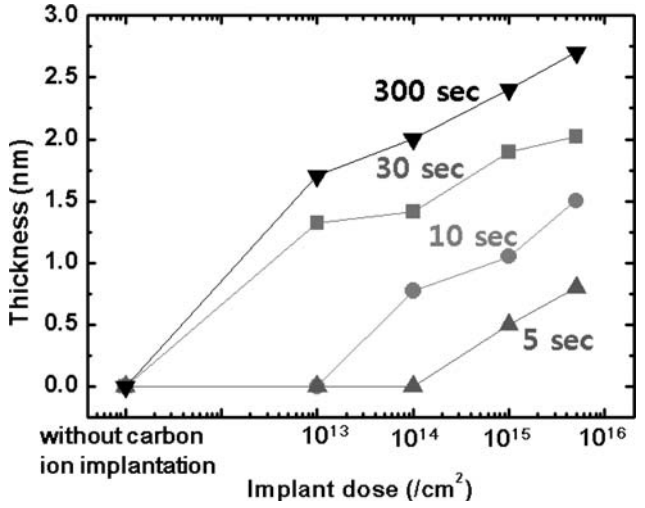

Figure 4. Average thickness of graphene layers for a wide range of implantation doses from 1×10^{13} to 5×10^{15} /cm^2 and various RTA time durations. The thickness was measured by AFM. The thicknesses of the samples without carbon implantation are also plotted.

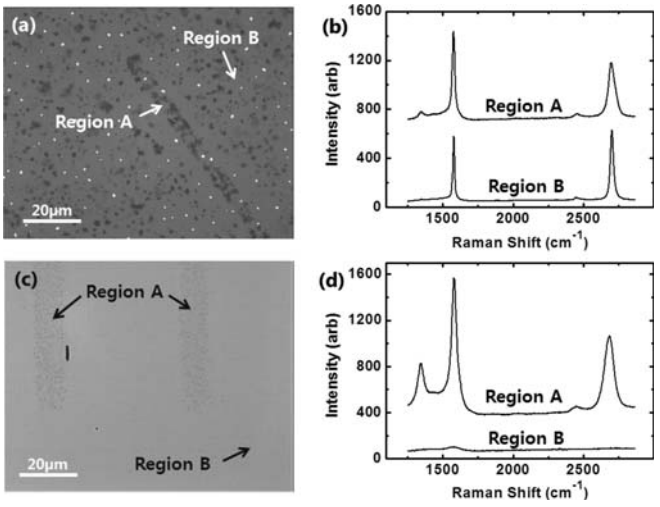

Figure 6. Microscope image of graphene layers after the local growth of graphene. The samples were annealed at (a) 800 mTorr in 10% H_2/Ar ambient, and (b) UHV ambient. (b) and (d) show the corresponding Raman spectra for the samples in (a) and (c), respectively.

thickness than the implantation dose. In addition, a graphene layer could be synthesized even at a dose much lower than an amount of the theoretically required. By a simple calculation considering the carbon atom density in the graphene layer, a carbon dose of at least 3.7×10^{15} /cm^2 is required for the formation of monolayer graphene. However, the experimental results show that graphene layers thicker than 1.7 nm are synthesized at an implantation dose of 1×10^{13} /cm^2 at a RTA time exceeding 30 sec. For an explanation of this phenomenon, unintentional adsorption of carbon atoms from ambient air on the nickel surface prior to the RTA step was initially suspected. To clarify this, several nickel samples without carbon implantation were exposed to ambient air for several days and then annealed under the same conditions used for graphene synthesis, after which they were transferred onto SiO_2(100 nm)/Si substrates for an evaluation of the thickness. However, no graphene layer was observed for any of the synthesis conditions. This indicates that the contamination from ambient air is not the source of the carbon for thick graphene formation. Thus, we speculate that once a small amount of implanted carbon is segregated on the nickel surface, it may provide nucleation sites; residual carbon in the chamber would then be absorbed onto the nucleation sites during the high-temperature RTA process.

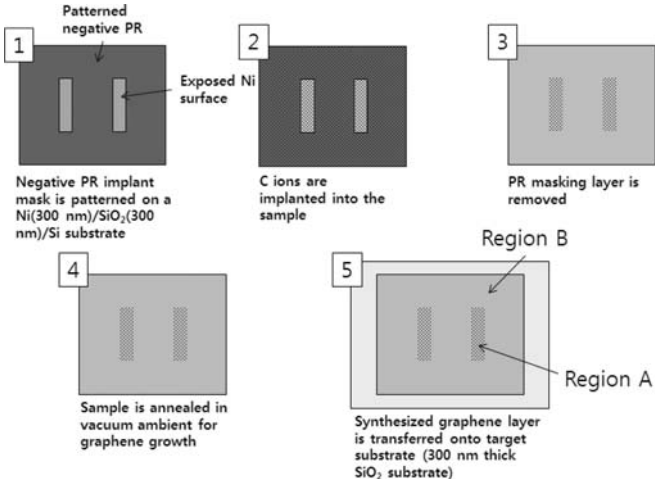

Figure 5. Illustration of process sequence for the local growth of graphene.

To clarify the observation of excessive growth of graphene with an insufficient implantation dose of carbon ions, graphene synthesis was conducted in a UHV (ultra-high vacuum) ambient atmosphere to examine the effects of carbon adsorption from the chamber environment. In this experiment, local implantation of carbon ions was carried out through photoresist patterns, as illustrated in Fig. 5. After the implantation of carbon atoms at an energy level of 40 keV and a dose of 5×10^{15} /cm^2, the photoresist was removed by dipping in acetone, methanol, and deionized water for 10 min for each step. Because there is possibility that the residual photoresist is a source of carbon, we prepared an additional Ni/SiO_2/Si sample with photoresist patterns but with no carbon implantation. After the same photoresist process and annealing, it was confirmed that no graphene was synthesized on this sample, indicating complete removal of the photoresist. For the graphene growth, the implanted samples were annealed at 800°C for 300 sec in 10% H_2/Ar ambient at a pressure of 800 mTorr. In the meantime, another sample was annealed under a UHV ambient at a base pressure of $\sim 2 \times 10^{-10}$ Torr with the same temperature profile. During the annealing process in the UHV chamber, the pressure was increased to $\sim 2 \times 10^{-8}$ Torr at a high temperature. The synthesized graphene layers were transferred onto a SiO_2(100 nm)/Si substrate. For easy identification, the notations "Region A" and "Region B" are used in Figs. 5 and 6. "Region A" is the region on which the carbon ions are implanted and "Region B" is the region where carbon implantation is blocked by the photoresist. The results for the local implantation and annealing are shown in Fig. 6. For the sample annealed in an H_2/Ar ambient, non-uniform thick graphene layers are synthesized over both regions, A and B, and the pattern is scarcely recognizable. For the sample annealed in the UHV ambient atmosphere, however, no graphene is observed in region B. In this sample, the graphene pattern in region A is also only faintly defined. It appears that the graphene layer is not continuous owing to insufficient carbon, which is also supported by the large D peak in region A (Fig. 6d). The results in Figs. 5 and 6 provide experimental evidence that the excessive growth of graphene after carbon implantation and RTA occurred due to additional carbon absorption from the chamber environment during RTA. This also shows that, in cases where local growth of graphene with a certain pattern is required, the sample must be annealed in a well-controlled ambient such as UHV. Moreover, the implantation dose must be sufficiently high.

Conclusions

We demonstrated the synthesis of monolayer graphene using a typical semiconductor chip manufacturing technique of carbon

implantation with a subsequent RTA process. The dependence of the process conditions, including the RTA temperature and the time as well as the implantation dose, on the graphene quality were investigated. The processing issue of local growth of graphene through local implantation was also discussed. The methodology presented here can provide an alternate means of graphene synthesis using traditional semiconductor process techniques. The method will also be useful for the local growth of graphene on a wafer, which is an important issue for graphene/silicon hybrid circuit fabrication.

Acknowledgment

This work was supported by the National Research Foundation of Korea (NRF) Research grant, 2008-2002744, 2010-0029132, and 2011-0031638.

References

1. K. S. Novoselov, A. K. Geim, S. V. Morozov, D. Jiang, Y. Zhang, S. V. Dubonos, I. V. Grigorieva, and A. A. Firsov, *Science*, **306**, 666 (2004).
2. K. S. Novoselov, A. K. Geim, S. V. Morozov, D. Jiang, M. I. Katsnelson, I. V. Grigorieva, S. V. Dubonos, and A. A. Firsov, *Nature*, **438**, 197 (2005).
3. Y. Zhang, Y. W. Tan, H. L. Stormer, and P. Kim, *Nature*, **438**, 201 (2005).
4. K. I. Bolotin, K. J. Sikes, Z. Jiang, M. Klima, G. Fudenberg, J. Hone, P. Kim, and H. L. Srormer, *Solid State Commun.*, **146**, 351 (2008).
5. Q. Yu, J. Lian, S. Siriponglert, H. Li, Y. P. Chen, and S. S. Pei, *Appl. Phys. Lett.*, **93**, 113103 (2008).
6. A. Reina, X. Jia, J. Ho, D. Nezich, H. Son, V. Bulovic, M. S. Dresselhaus, and J. Kong, *Nano Lett.*, **9**, 30 (2009).
7. K. S. Kim, Y. Zhao, H. Jang, S. Y. Lee, J. M. Kim, K. S. Kim, J. H. Ahn, P. Kim, J. Y. Choi, and B. H. Hong, *Nature*, **457**, 706 (2009).
8. X. Li, W. Cai, J. An, S. Kim, J. Nah, D. Yang, R. Piner, A. Velamakanni, I. Jung, E. Tutuc, S. K. Banerjee, L. Colombo, and R. S. Ruoff, *Science*, **324**, 1312 (2009).
9. Y. Lee, S. Bae, H. Jang, S. Jang, S. E. Zhu, S. H. Sim, Y. I. Song, B. H. Hong, and J. H. Ahn, *Nano Lett.*, **10**, 490 (2010).
10. A. Reina, S. Thiele, X. Jia, S. Bhaviripudi, M. S. Dresselhaus, J. A. Schaefer, and J. Kong, *Nano Res.*, **2**, 509 (2009).
11. S. Bae, H. Kim, Y. Lee, X. Xu, J. Park, Y. Zheng, J. Balakrishnan, T. Lei, H. R. Kim, Y. I. Song, Y. J. Kim, K. S. Kim, B. Ozyilmaz, J. H. Ahn, B. H. Hong, and S. Iijima, *Nat. Nanotech.*, **5**, 574 (2010).
12. Q. Yu, L. A. Jauregui, W. Wu, R. Colby, J. Tian, Z. Su, H. Cao, Z. Liu, D. Pandey, D. Wei, T. F. Chung, P. Peng, N. P. Guisinger, E. A. Stach, J. Bao, S. S. Pei, and Y. P. Chen, *Nat. Mat.*, **10**, 443 (2011).
13. J. Hofrichter, B. N. Szafranek, M. Otto, T. J. Echtermeyer, M. Baus, A. Majerus, V. Geringer, M. Ramsteiner, and H. Kurz, *Nano Lett.*, **10**, 36 (2010).
14. Z. Y. Juang, C. Y. Wu, C. W. Lo, W. Y. Chen, C. F. Huang, J. C. Hwang, F. R. Chen, K. C. Leou, and C. H. Tsai, *Carbon*, **47**, 2026 (2009).
15. C. M. Orofeo, H. Ago, B. Hu, and M. Tsuji, *Nano Res.*, **4**, 531 (2011).
16. M. Zheng, K. Takei, B. Hsia, H. Fang, X. Zhang, N. Ferralis, H. Ko, Y. L. Chueh, Y. Zhang, R. Maboudian, and A, Javey, *Appl. Phys. Lett.*, **96**, 063110 (2010).
17. S. Garaj, W. Hubbard, and J. A. Golovchenko, *Appl. Phys. Lett.*, **97**, 183103 (2010).
18. L. Baraton, Z. He, C. S. Lee, J. L. Maurice, C. S. Cojocaru, A. F. G. Lorenzon, Y. H. Lee, and D. Pribat, *Nanotech.*, **22**, 085601 (2011).
19. D. Graf, F. Molitor, K. Ensslin, C. Stampfer, A. Jungen, C. Hierold, and L. Wirtz, *Nano Lett.*, **7**, 238 (2007).
20. A. C. Ferrari, J. C. Meyer, V. Scardaci, C. Casiraghi, M. Lazzeri, F. Mauri, S. Piscanec, D. Jiang, K. S. Novoselov, S. Roth, and A. K. Geim, *Phys. Rev. Lett.*, **97**, 187401 (2006).